Experimental Validation of CFD simulations of Free-Fall Lifeboat Launches in Regular Waves

Nabila **Berchiche**
Nabila.Berchiche@marintek.sintef.no
Anders **Östman**
Anders.Ostman@marintek.sintef.no
Ole Andreas **Hermundstad**
Ole.Hermundstad@marintek.sintef.no
Tel: +47 41608840
(Corresponding author)

MARINTEK
Norwegian Marine Technology Research Institute,
P.O.Box 4125 Valentinlyst
NO-7450 Trondheim, Norway

Svein-Arne **Reinholdtsen**
SveRei@statoil.com

STATOIL, Norway

Abstract

The loads on a free-fall lifeboat and the accelerations felt by the occupants during water-entry are influenced by a large number of parameters: drop height, presence of wind and waves, location of impact point relative to the wave crest. Therefore, testing the lifeboat design and performance by means of experiments becomes difficult and costly. Furthermore, the most critical conditions are not even possible to reproduce experimentally, due to the lifeboat's small size relative to the most severe waves. However, numerical simulations of lifeboat launching under different conditions are possible with the newly developed models in Computational Fluid Dynamics (CFD) solvers. In addition, CFD provides more data that can be used to improve the hull design.

This paper presents results from new model tests and CFD simulations of lifeboat launches in oblique regular waves from 3 different directions. To the authors' knowledge, this is the first time CFD simulations of lifeboat launches in waves have been validated. The predicted accelerations of the lifeboat agreed well with the measured ones. The pitch velocity was slightly overestimated due to a slight difference in the geometric features at the bow between the CFD model and the physical model. The CFD simulations provided in general accurate or conservative estimates of the local pressure at various locations on the hull except on one location on top of the canopy where the pressure was slightly under-predicted. Furthermore, it has been shown that to improve the predictions of the pressure loads on the aft wall of the lifeboat, the compressibility of air has to be taken into account in the CFD simulations in order to capture the behavior of the air-pocket behind the lifeboat.

Key words: Lifeboat, CFD, pressure, validation, waves

1 Introduction

Free-fall lifeboats serve as the evacuation system for fixed and floating offshore installations in conditions where helicopter evacuation is not possible. These lifeboats are installed at a height of typically 20 to 30 meters above the sea level, and they are launched by dropping

them vertically or by sliding them on a 35 degree skid for a few meters before they enter into free fall. In recent years significant efforts have been devoted to the assessment of the performance of free-fall lifeboats on the Norwegian continental shelf. The performance assessment focuses on the loads and structural integrity (Tregde and Nestegård 2013), the accelerations and human responses (Sauder and Fouques 2009; Luxcey et al. 2010; Fouques et al. 2013, 2014) and the lifeboat's ability to escape from the installation in large waves and wind without collision (Tregde and Nestegård 2014; Jin et al. 2014). Numerical simulations, and sometimes model tests, are used in these studies. The lifting operation of a free-fall lifeboat during installation was simulated by Rønning et al (2011).

A free-fall lifeboat that is launched from a skid goes through many different phases, where the external forces are quite different. First, the boat slides on the skid for a few seconds. Then it rotates around the tip of the skid before it enters into free fall. During free fall it is exposed to gravity and wind forces. Next, the boat enters the wave surface with the bow first; normally with a pitch water entry angle (WEA) of 50-60 degrees. During this water entry phase, the boat experiences large slamming pressures that propagate from the bow to the stern and from the bottom to the superstructure (canopy). These pressures govern the design of the local hull structure. Depending on the WEA, the boat will normally rotate in pitch during this phase, and this increases the slamming pressures on the hull bottom aft. When the stern of the boat is passing the water surface it leaves an air cavity behind the boat. Subsequently, this cavity is being closed by the water and an air cavity is then entrapped behind the boat, which is now completely submerged. Then the air cavity collapses, causing large impact pressures on the stern of the boat. After the boat has reached its maximum submergence it starts the ascent phase. The boat is now subjected to large hydrostatic forces which may cause deformation to the boat's cross section. The next phase is water exit, and the propeller is either running or the helmsman shall activate the propeller and sail away without colliding with the host structure or other obstacles. In the sail-away phase the boat is subjected to waves wind and current.

Assessment of the lifeboat's motions and accelerations from it is released from the host installation and until it is completely submerged in the waves can generally be sufficiently well predicted by computationally efficient 6 degree-of-freedom models using wind-coefficients for the wind forces and hydrodynamic coefficients for the water entry forces (momentum theory); see Sauder and Fouques 2009. However, for the proper assessment of the pressure distribution around the hull and superstructure CFD simulations are required. CFD is also presently the preferred tool for assessment of the motions of the boat after the end of the water entry phase, and until the start of the sail-away phase.

The present paper focuses on the assessment of motions and pressure loads on free-fall lifeboats from water entry and until water exit using CFD simulations. The results are validated against new experimental data from model tests in waves and from full-scale tests in calm water. Validation of launch simulations by CFD has previously been presented for launches in calm water (e.g. Mørch et al. 2008; Tregde et al. 2011), but to the authors' knowledge, this is the first time CFD simulations of lifeboat launches *in waves* have been validated.

2 Lifeboat Characteristics, Model tests and simulated drop cases

The main characteristics of the lifeboat at model-scale are given in Table 1. The physical model was tested in MARINTEK's towing tank. The model was equipped with a dummy propeller and nozzle. Slamming forces were measured on 4 circular panels, with diameter 57 mm, mounted flush with the exterior hull surface; see Figure 1 and Figure 2. The force transducers were equipped with accelerometers measuring the acceleration normal to the panel. This was used to remove the force component due to inertia in the panel-transducer system, so that the external force on the panel could be derived. In this paper, the panel-transducer system is simply referred to as a probe or pressure probe. Additional measurements were accelerations in x- y- and z-directions aft and forward as well as roll, pitch and yaw velocities. The release mechanism for the lifeboat was synchronized with a wave gauge so that the lifeboat could impact the wave surface at specified locations (hit-points) relative to the wave crest. The definition of the hit-points, denoted as HP, is shown in Figure 3. Data was transferred from the model via a thin optical fiber. Accelerations and rotation rates were sampled and filtered at 2400 Hz and 500 Hz, respectively, whereas slamming forces were sampled and filtered at 4800 Hz and 1000 Hz, respectively. During post-processing the accelerations and rotations were low-pass filtered at 20 Hz and the derived slamming forces were low-pass filtered at 22 Hz. The slamming forces were divided by the panel area to obtain a space-averaged pressure.

The mass of the model corresponded to a fully loaded boat. Due to the use of two different battery types, the mass properties of the model were not the same throughout the test program; see Table 1. In the present paper we will focus on tests were the boat was launched from a height of 3 m into regular waves coming from three different directions: beam (90 deg), bow quartering (60 deg) and stern quartering (120 deg). Figure 4 illustrates the orientation of the lifeboat relative to the waves for the three headings. In all simulated cases, the waves were propagating towards the port-side of the life-boat. The waves had a period of 2.58 s and a height of 0.75 m. This means that the wave was 8.65 times longer than the lifeboat and the wave steepness was 0.07. The investigated cases are summarized in Table 2. For each case, three launches were carried out. The repeatability of the tests was generally good. However, some scatter was observed partly due to small variations in the hit-point. The samples selected for the comparison with CFD simulations were those which were closest to the specified hit-points.

In a real storm situation there will also be wind and current present, and the waves will be irregular. The wind will change the attitude of the boat during free fall and hence change the impact angle. This has been the focus of previous studies (Sauder et al 2014). Wind and current will also influence the performance of the boat when sailing away after the launch phase. This has been studied by e.g. Jin et al (2014). Since the focus of the present study is on validation of motion and pressure-predictions by CFD during impact in waves, it was decided to exclude wind and current from the experiments and to use regular waves. This improves the repeatability of the experiments and allows for a better understanding of the physics and the error sources.

3 Numerical set-up

3.1 CFD Method

The present simulations were run in the commercial CFD software STAR-CCM+ developed by CD-adapco. Unsteady Reynolds-Averaged Navier-Stokes (RANS) equations were solved using a finite volume discretization method to simulate lifeboat drops in regular waves. The implicit unsteady model was used with a second order temporal discretization. The flow was set as laminar and both water and air phases were considered incompressible. The water-air interface was resolved with the Volume of Fluid (VOF) multiphase model. The waves were simulated using the VOF waves model and were described as first-order Stokes waves with regular periodic sinusoidal profile. One case (Case1) has been simulated also with the fifth-order Stokes-waves since it exhibits a more realistic wave profile than the one generated by the first-order approximation.

3.2 Motion Model and Computational Mesh

The simulations were performed using the Dynamic Fluid Body Interaction (DFBI) embedded rotation model in which the lifeboat is placed in a sphere and is free to move in all six rigid-body motion modes. Details about this motion model can be found in STAR-CCM+ User's Guide. The entire computational domain consisted of two regions connected with an internal sliding interface: a sphere containing the lifeboat and an outer-rectangular domain that translates in three directions following the motion of the lifeboat, Figure 5. The length, width and height ratios of the domain relative to the length of the boat were about 16.5, 4.5 and 5.25 respectively. The total length of the domain corresponded to about twice the wave-length. This type of simulation can be solved using either the embedded rotation model described briefly above or the overset model that consists of two overlapping regions: a stationary background domain and a sub-domain containing the moving lifeboat. The selection of the embedded model is due to the fact that it requires less grid cells and therefore a reduced computational time compared to the overset model. Two cases were run also with the overset model and the results were similar to the ones computed with the embedded rotation model.

The mesh generated for the present simulations consisted predominantly of hexahedral cells with trimmed cells at locations where the grid intersects with the surface of the geometry. A prism layer was placed around the hull. The total grid size was approximately 2.6 million cells with 2.02 million cells located within the sphere. The mesh on the hull surface was further refined on the pressure probes as illustrated in Figure 6. The mesh was created with the lifeboat at its horizontal position. To set the lifeboat at a given orientation, only the mesh in the sphere was rotated.

The geometry modelled in the CFD simulations was slightly different from the one used in the model tests, particularly at the bow. An edge was present in the CFD model, while the physical model had a smoother bow.

The global "earth-fixed" coordinate system adopted in STAR-CCM+ is right-handed, with x-axis pointing to North, y-axis to West and Z-axis pointing upwards. The origin of the local coordinate system fixed to the lifeboat lies at its center of gravity and is defined as follows: x-axis points towards the bow, y-axis towards the starboard and z-axis towards the keel.

The boundary conditions were the following: a velocity inlet was specified on the inlet, top and bottom boundaries as well as on the two side-boundaries parallel to the wave propagation direction, Figure 5. A pressure outlet was assigned on the outlet boundary and a no-slip wall condition was specified on the lifeboat surface.

4 Results and Discussion

The CFD simulations performed in this study were water-entry simulations that started shortly before the water impact. The initial positions and velocities prior to impact were taken from model test data. In this section, results from the CFD simulations are compared against model test results. This comparison is shown only for the selected cases: Case 1, Case 7 and Case 11, i.e. one case for each wave heading. Case 1 is the case that showed the largest discrepancies between the numerical predictions and model tests. Case 7 and Case 11 resulted in the highest pressure levels for a wave heading of 60 and 120 degrees respectively. In the comparison, the time-histories of the linear accelerations at the center of gravity, the pitch velocity (angular y-velocity) in the body-fixed coordinate system and the surface-averaged pressure on the probes are considered.

Figure **7** illustrates the computed and measured accelerations and pitch velocity for the selected cases. The numerical simulations seem to predict higher values of the maximum magnitude of the z-acceleration and pitch velocity, but the overall shape of the plots with accelerations and pitch velocities compare rather well to the measurements. The larger value of the maximum pitch velocity in CFD can be partly related to the presence of an edge in the bow area of the CFD model, which was not present on the physical model. The effect of the bow geometry has been investigated for a calm water case. A simulation was performed with a smoother bow geometry (closer to that of the physical model) and this resulted in a better prediction of the maximum pitch-velocity, as shown in Figure 9.

Figure 8 illustrates the computed and measured surface-averaged pressure on all four probes for the selected cases. In general, the computed pressures on probes P1 and P2 agree very well with the measured pressures except for Case 1, where the computed pressure on P1 is over-predicted.

The pressure is under-predicted on P3 and over-predicted on P4. The difference between the measured and computed pressures is greater on P4, probably due to the fact that P4 is located close to the stern where the effect of the "closing" air-pocket behind the lifeboat is higher. The over-prediction of the pressure on P4 is most pronounced after the bottom of the lifeboat hits the water surface as observed particularly in Case 1. The first part of the pressure plot for P4, which corresponds to the slamming phase, is quite well captured by the CFD simulation, although an over-prediction of the slamming peak can be noticed, and this is probably due to the over-prediction of the pitch velocity. The two pressure plots start deviating from each

other shortly after the stern has hit the water surface and the deviation increases when the air-pocket has formed behind the lifeboat. The time at which the air-pocket is formed can be identified from the time-history of the x-acceleration. Figure 7 depicts a sharp pulse that occurs at about 0.39 s for Case 1, which corresponds to the moment the air-pocket behind the lifeboat closes. A sharp pulse is also visible on the pressure time-history on P4 at the same time instance. This time can also be detected on the pressure plots of P1, P2 and P3 but the pulses are less prominent since these probes were located further away from the aft part of the lifeboat. In the present simulation, the air-phase was considered incompressible. Taking into account the compressibility of the air in the CFD simulations is expected to capture the behavior of the air-pocket more properly and improve the predictions. The effect of compressibility has been investigated for a different lifeboat tested in calm-water at full-scale. The results of this study are presented in the next section.

Case 1 has also been run with a finer grid with approximately 3.6 million cells to check whether an increase of grid resolution would improve the results. The aim of the refinement was not to investigate the order of the numerical scheme. Instead the purpose was to perform local refinements to better capture areas with large gradient in the flow field. The mesh was therefore only refined within the sphere region and not in the outer-domain. In particular, at the surface of the vessel, the mesh near the flange connecting the hull and canopy was refined significantly. Also, in order to better capture the rapid and dramatic evolution of the free surface close to the lifeboat during the drop, the volume mesh was refined in the vicinity of the lifeboat. Within a distance from the lifeboat surface, corresponding to approximately 50% of its transverse dimensions, the grid cell density was approximately doubled compared to the original mesh. Results obtained with the original and the refined meshes are presented in Figure 10 and Figure 11, and it is seen that the differences in computed accelerations at COG, pitch velocity and surface-averaged pressure are very small. Similar observations are made when comparing the results obtained with the first-order and fifth-order stokes waves. Although the difference in computed results using first order and higher order modeling of the wave was small in the present case, this is not necessarily true for all launch events. Our general recommendation is to use a numerical modeling of the wave which is as close as possible to the real wave.

Furthermore, it has been observed both in CFD results and model tests that:

- for a wave heading of 90 degrees, the largest accelerations occurred for Case 3 (HP2), where the boat hits the wave trough. However, the highest local pressures occurred for Case 2 (HP1).

- for a wave heading of 60 degrees, the largest accelerations occurred for Case 6 (HP1) while the highest local pressures occurred for Case 7 (HP2).

- and for a wave heading of 120 degrees, the largest accelerations occurred for Case 10 (HP1) and the highest local pressures occurred for Case 11 (HP2).

These observations suggest that, for the given wave headings, the most critical conditions for this particular lifeboat in terms of accelerations and loads are the conditions in which the lifeboat hits the wave in the area between hit point 2 (corresponding to the wave trough) and hit point 1 (corresponding to the steepest part of the wave profile with water velocity upward).

5 Effect of compressibility on the computed pressure loads at Full-scale

This section compares results of CFD simulation of lifeboat drop in calm water with full-scale test data. The main quantities considered in this validation study are: the linear accelerations, pitch velocity and surface-averaged pressure at seven different locations on the hull. The pressure probes are indicated by the circles in Figure 12. The probes have approximately the same surface area as those used during the model tests described in the previous section. Hence, their size relative to the lifeboat is much smaller than for the model test probes. The simulation was performed using the embedded rotation model. The total grid size was approximately 1.88 million. The number of cells within the sphere was about 1.54 million. The initial positions and velocities prior to impact were taken from full-scale test data.

Figure 13 and Figure 14 contain results of the CFD simulations together with full-scale data for two tests (denoted Test 1 and Test 2) performed in identical conditions. The input parameters for the CFD simulations (initial position and velocities just before water impact) were taken from Test 1. The predictions of accelerations and pitch velocity compare reasonably well to full-scale tests results.

The computed pressures on the probes agree quite well with the measured pressures except for probes P5, P6 and P8. The negative pressure peaks observed in the measurements for probes P4 and P7 are probably caused by inertia effects due to the large local acceleration of the hull surface deflection under the high and localized slamming peak. The hull is considered completely rigid in the CFD simulations.

On probes P5 and P6, the pressure is under-predicted. This is partly due to the fact the computed flow is slightly different from that in the full-scale tests due to the presence of rails and other details on the hull surface. In the CFD simulations, the lifeboat was represented by a bare hull only.

Even though the maximum pressure level on P8 is reasonably well predicted, the shape of the pressure plot is rather different from the one measured during the full-scale tests. The computed rise-time of the pressure at P8 is very short compared to the experiments. Probe P8 was located on the aft wall of the lifeboat where the effect of the "closing" air-pocket is predominant. In the present simulation, the air was considered incompressible. By taking into account the compressibility of the air in the simulation, the shape of the computed pressure at P8 has been notably improved, as shown in Figure 15. Based on these results, it is evident that compressibility has to be included in the CFD simulations in order to make a proper prediction of the pressure on the aft-wall of the lifeboat and anywhere else where air is entrapped.

6 Conclusions

Simulations of water entry of a free-fall lifeboat into waves of different directions have been performed with the STAR-CCM+ software and validated against results from model tests. The following conclusions can be made:

- The CFD simulations were able to predict the motions of the lifeboat during water entry into waves of various directions.
- The accelerations and angular velocities of the lifeboat were well predicted, and this indicates that the global forces and moments caused by the fluid actions were also well predicted.
- The computed pressures on panels located at different positions on the hull compared quite well to the measured values during model tests.
- The accelerations and the trajectory of the lifeboat, as well as the pressure distribution on most parts of the lifeboat, were well predicted when the air was modelled as incompressible. However, it has been shown that for a proper prediction of local pressures at places where air-cavities are formed and then collapse, such as at the aft wall of the lifeboat, it is necessary to model the air as compressible.

7 Acknowledgements

This work has been performed within projects funded by Statoil ASA and Norsafe AS.

The authors thank their colleagues at MARINTEK, Wojciech Kauczynski and Sébastien Fouques, for providing all the experimental data needed for the validation.

8 References

CD-adapco, User's Guide, STAR-CCM+ Version 7.02.011, 2012.

Fouques, S., Croonenborghs, E., Aksnes, V., Luxcey, N., Reinholdtsen, S. and Jokstad, C.I. 2013. Establishment of operational criteria for safe launch of free-fall lifeboats from a turret-moored FPSO, Proc. OTC Brazil 2013, Paper no. OTC-24402-MS.

Fouques, S., Sauder, T., Reinholdtsen, S., van Dam, E. and Uittenbogaard, J. 2014. Human Injury probability during water entry of free-fall lifeboats: Operational criteria based on long-term simulations using hindcast data, Proc. OMAE 2014, Paper no. 24074.

Jin, J., Ringen, E., Östman, A., Sauder, T., Hermundstad, O.A., Fathi, D. and Reinholdtsen S. 2014. Forward distance performance of free fall lifeboat in a sea way, Proc. ISOPE 2014, Busan, Korea.

Luxcey, N., Fouques, S. and Sauder, T. 2010. Computing acceleration loads on free-fall lifeboat occupants: Consequences of including nonlinearities in water waves and mother vessel motions, Proc. OMAE 2010, Paper no. 20329.

Mørch, H. J., Enger, S., Peric, M. and Schreck, E. 2008. Simulation of flow and motion of lifeboats, Proc. 6th Int. Conf. on CFD in Oil & Gas, Metalurgical and Process Industries, Trondheim, Norway.

Rønning, L., Heggernes, K. Nilsen, J.O. and Lie, H.B., 2011. A methodology for simulating safe offshore installation of lifeboats in the north sea. Trans. SNAME Vol. 119, pp 299-313.

Sauder, T. and Fouques, S., 2009. Theoretical study of the water entry of a body in waves. Application to safety of occupants in free-fall lifeboats, Proc. OMAE 2009, Paper no. 79981.

Sauder, T., Croonenborghs, E., Fouques, S., Berchiche, N and Reinholdtsen, S.-A. 2009. Effect of wind loads on the performance of free-fall lifeboats, Proc. OMAE 2014, Paper no. 24456.

Tregde, V., Halvorsen, T.E. and Underhaug, K.O. 2011. Simulation of free fall lifeboats – impact forces, slamming and accelerations, Proc. 11th Int. Conf. on Fast Sea Transportation – FAST2011, Honolulu, USA

Tregde, V. and Nestegård, A. 2013. Statistical methods for prediction of characteristic loads for free fall lifeboats based on CFD screening results, Proc. OMAE 2013, Paper no. 10296.

Tregde, V. and Nestegård, A. 2014. Predictions of irregular motions of free-fall lifeboats during drops from damaged FPSO, Proc. OMAE 2014, Paper no. 23090.

Figure captions

Figure 1. Left: Model during launch. Right: Slamming panels (pressure probes).

Figure 2. Location of the pressure probes on the hull.

Figure 3. Definition of hit point in regular waves.

Figure 4. Orientation of the lifeboat relative to the waves for different heading angles.

Figure 5. View of the computational domain (Wave propagating in x-direction).

Figure 6. Surface mesh on the hull.

Figure 7. Computed and measured time-histories of linear accelerations and pitch velocity for cases 1, 7 and 11.

Figure 8. Computed and measured time-histories of the surface-averaged pressure on all probes for cases 1, 7 and 11. See Figure 2 for location of the propes P1-P4.

Figure 9. Effect of the bow geometry on the computed pitch velocity for a calm-water case.

Figure 10. Effect of grid resolution on the computed time-histories of the surface-averaged pressure for Case 1.

Figure 11. Effect of grid resolution on the computed accelerations and pitch velocity for Case 1.

Figure 12. Location of the pressure probes during the full-scale tests.

Figure 13. Computed and measured time-histories of x-acceleration, z-acceleration and pitch velocity.

Figure 14. Computed and measured time-histories of the surface-averaged pressure on all probes. See Figure 12 for location of the probes P1-P8.

Figure 15. Effect of compressibility on the computed pressure on the aft-wall of the lifeboat.

Table captions

Table 1. Main Characteristics of the Model-scale lifeboat.

Table 2. Simulated Drop Cases, Launch height: 3 m

Figures

Figure 1

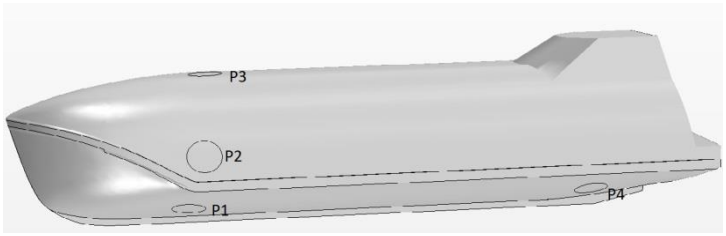

Figure 2

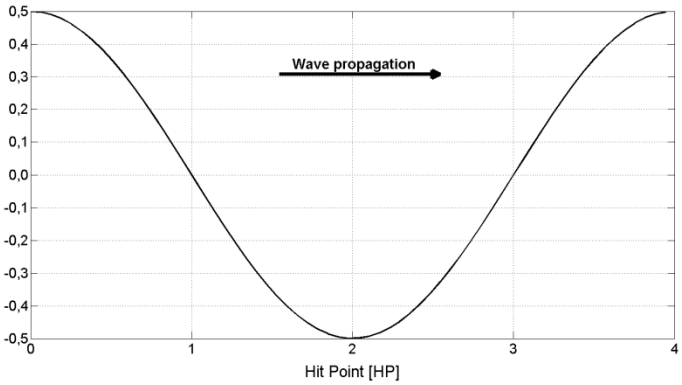

Figure 3

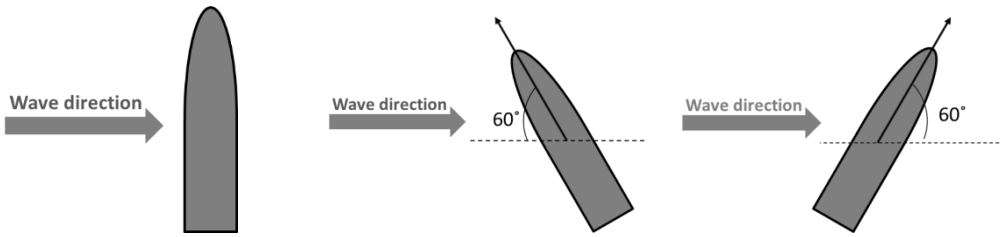

Wave heading 90 deg Wave heading 60 deg. Wave heading 120 deg.

Figure 4

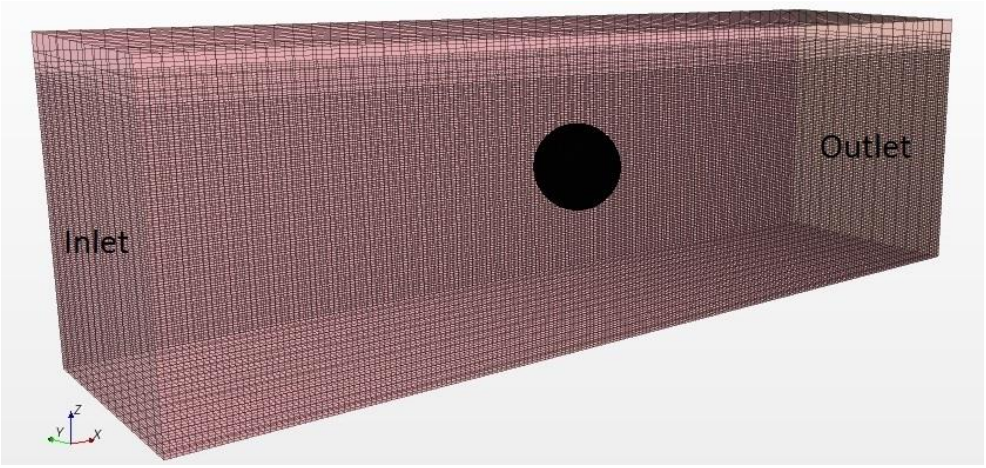

Figure 5

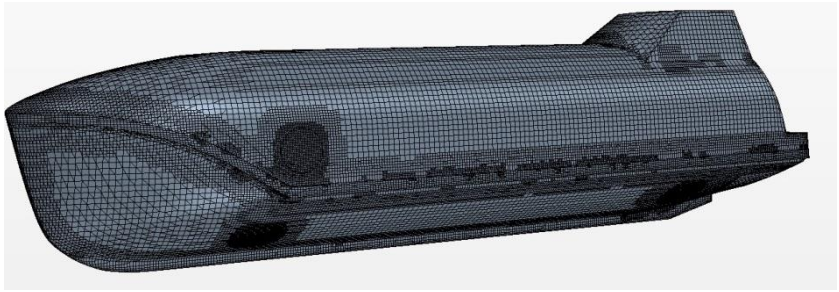

Figure 6

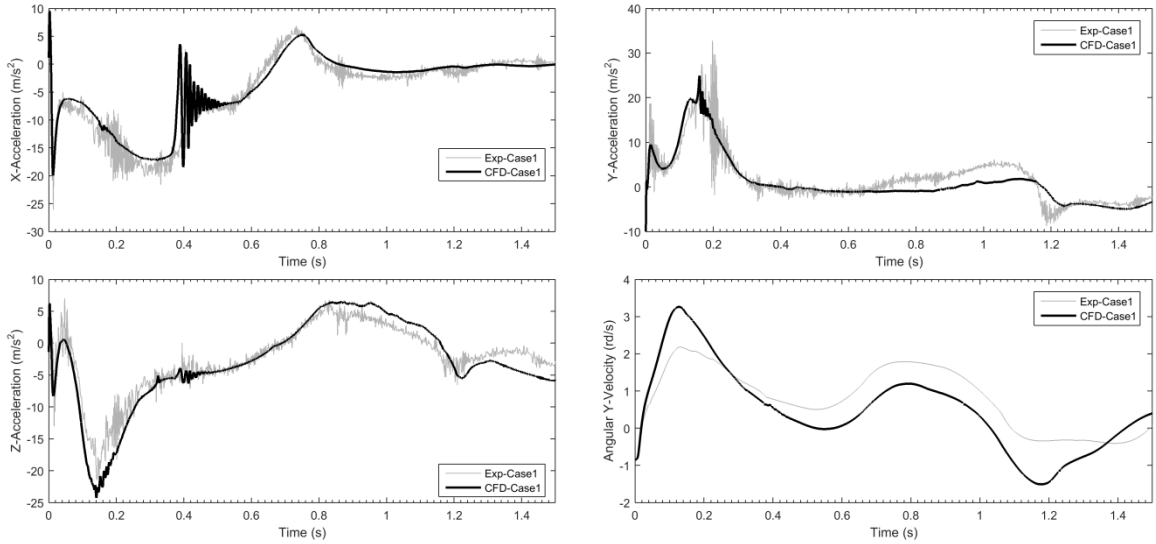

Case 1 (Wave heading 90 degrees, HP0)

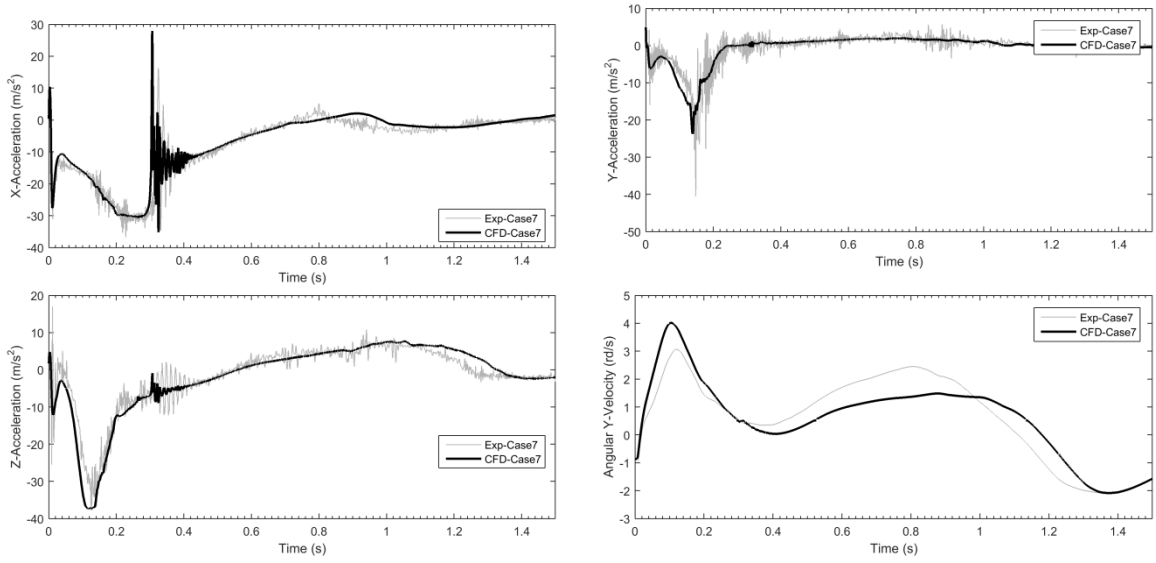

Case 7 (Wave heading 60 degrees, HP2)

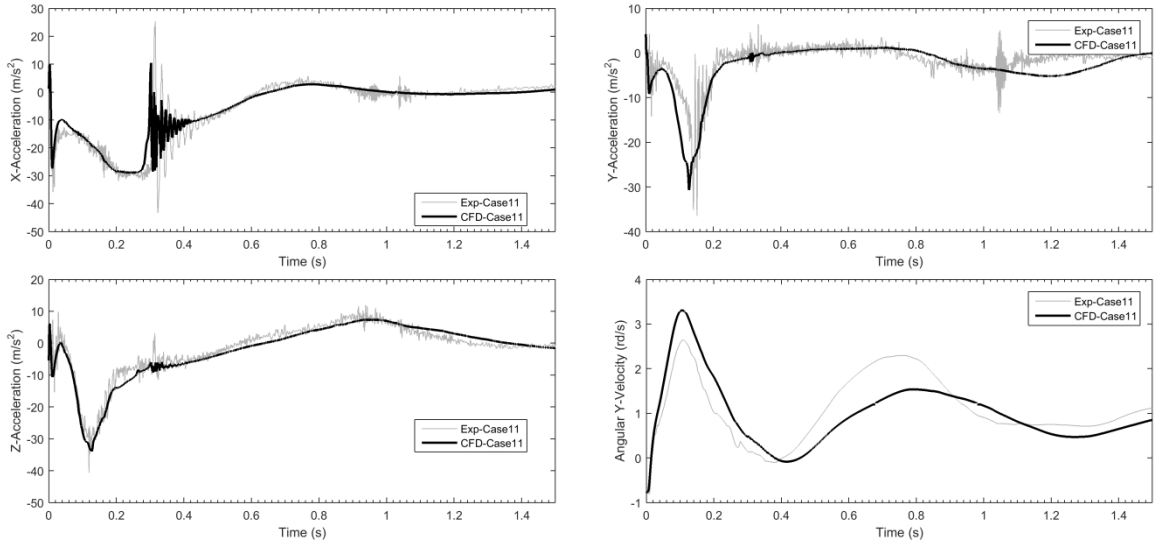

Case 11 (Wave heading 120 degrees, HP2)

Figure 7

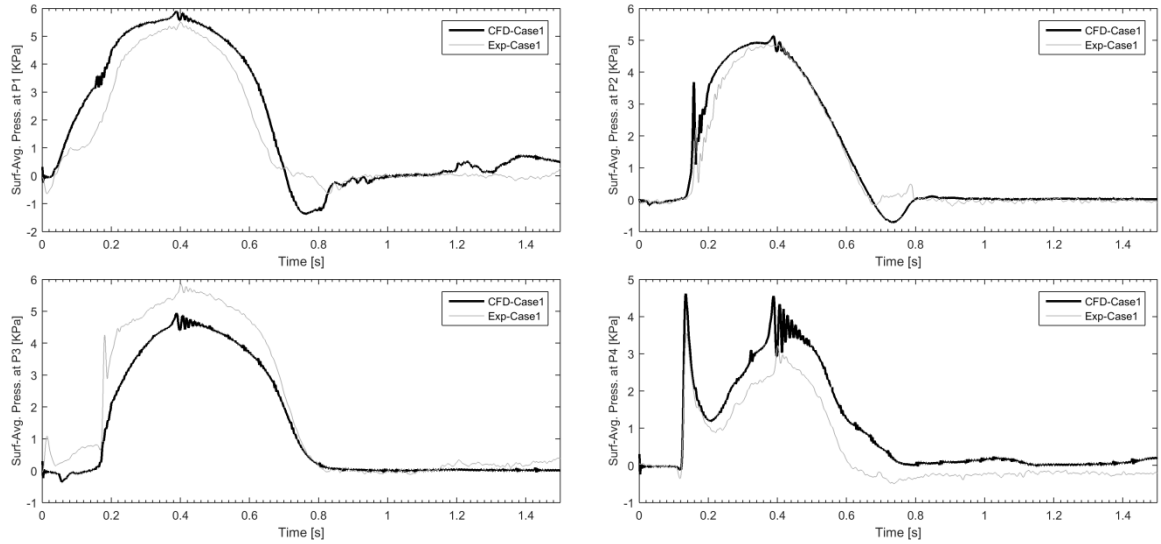

Case 1 (Wave heading 90 degrees, HP0)

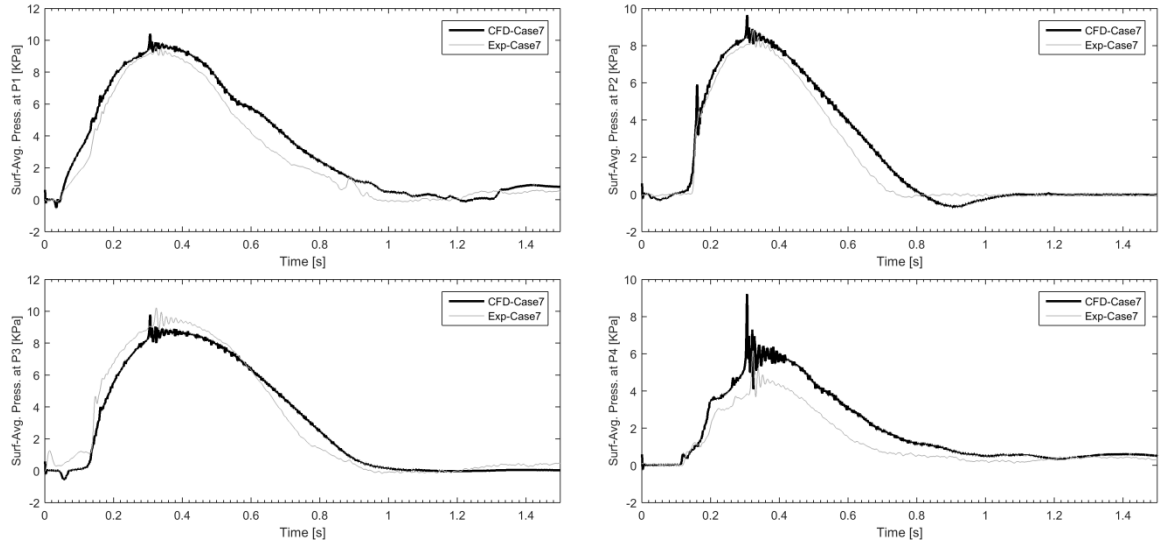

Case 7 (Wave heading 60 degrees, HP2)

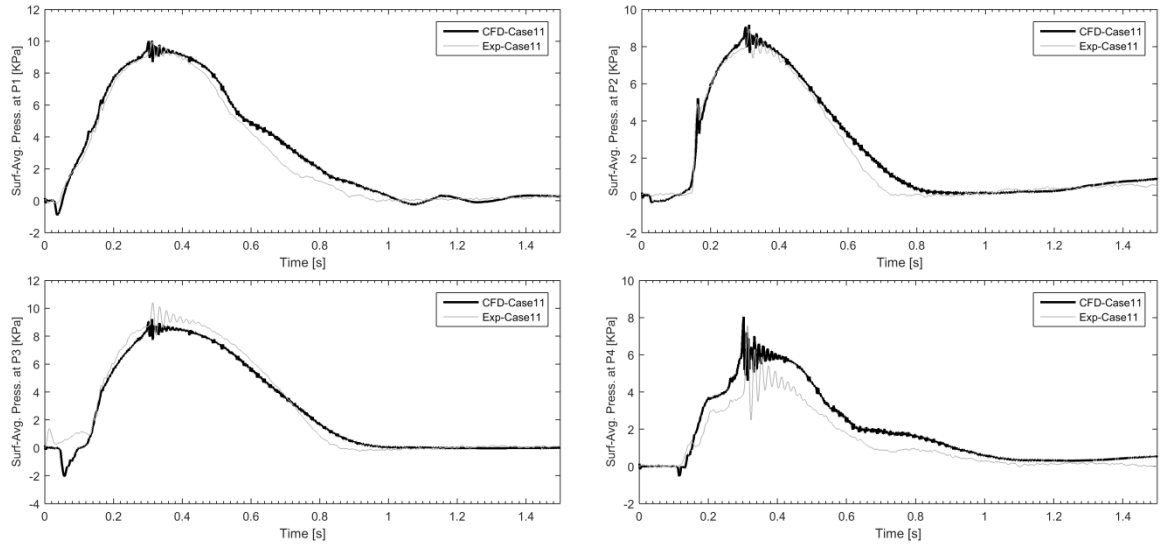

Case 11 (Wave heading 120 degrees, HP1)

Figure 8

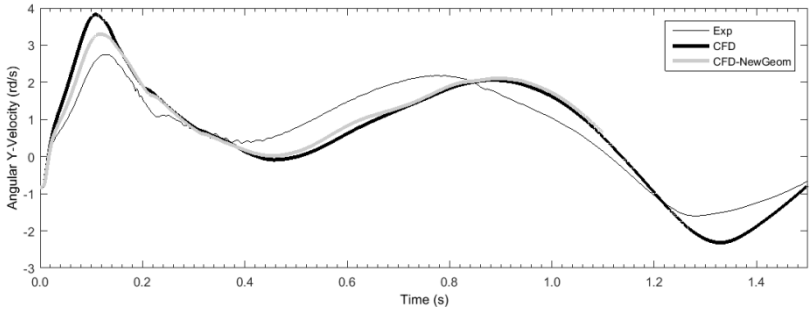

Figure 9

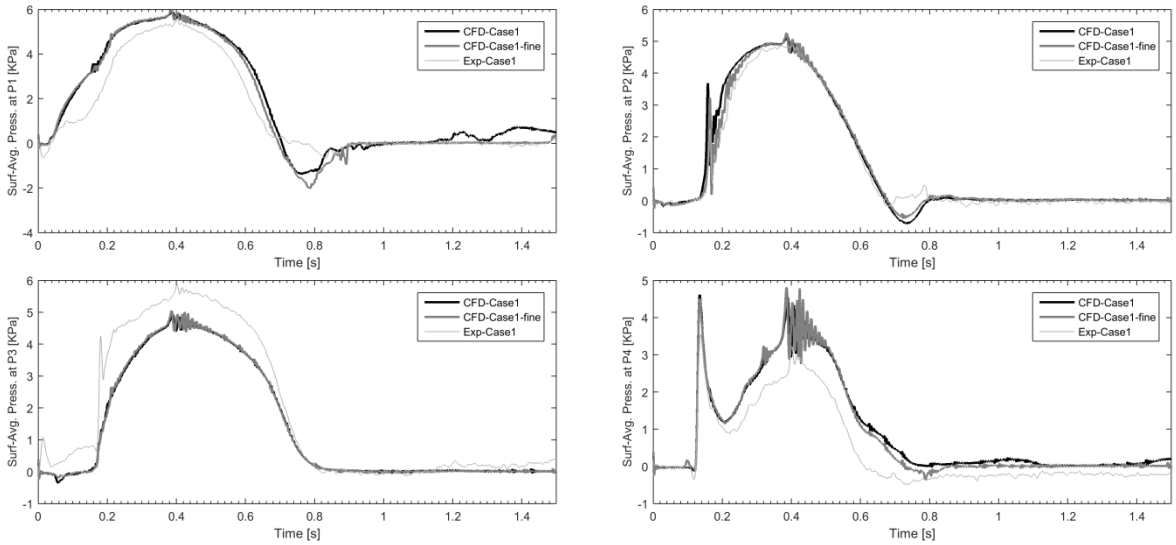

Figure 10

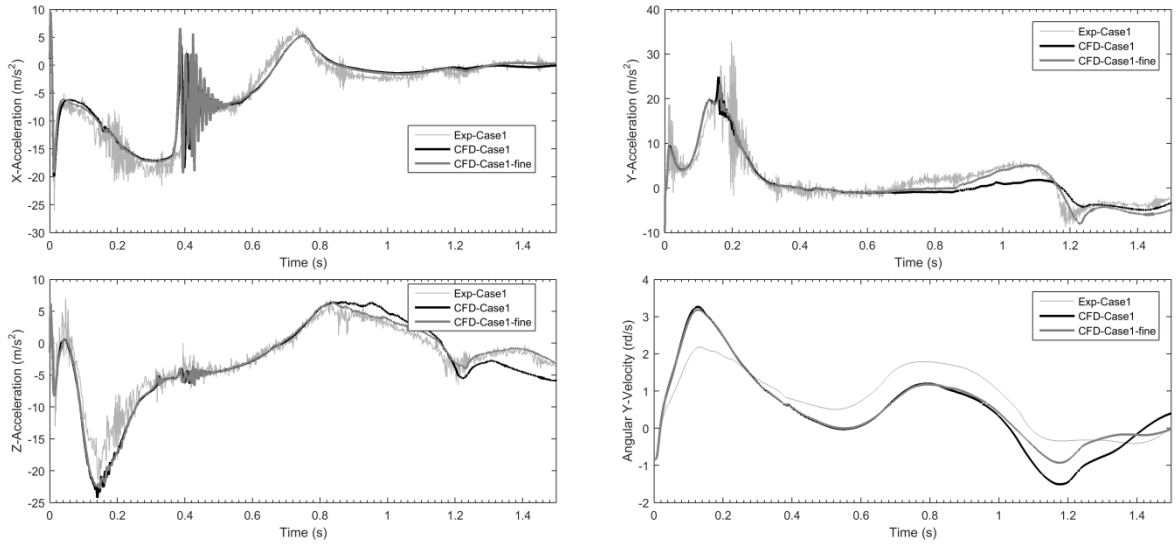

Figure 11.

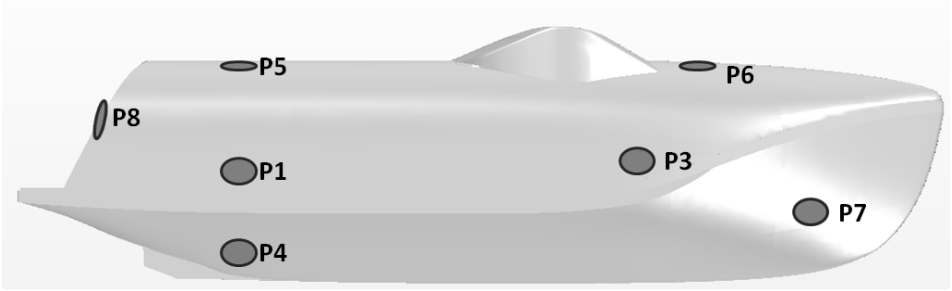

Figure 12

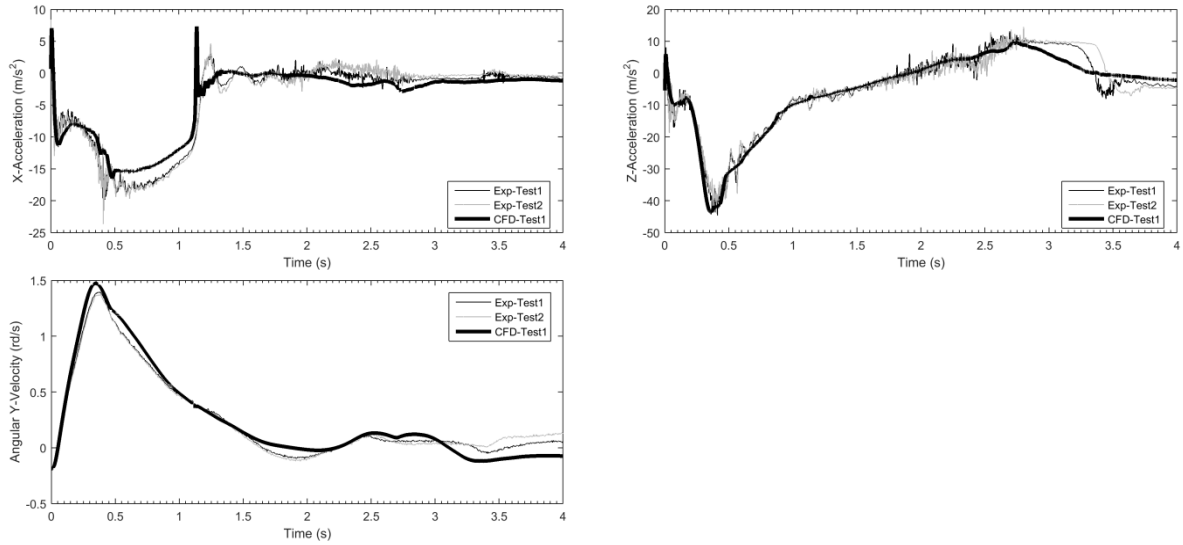

Figure 13

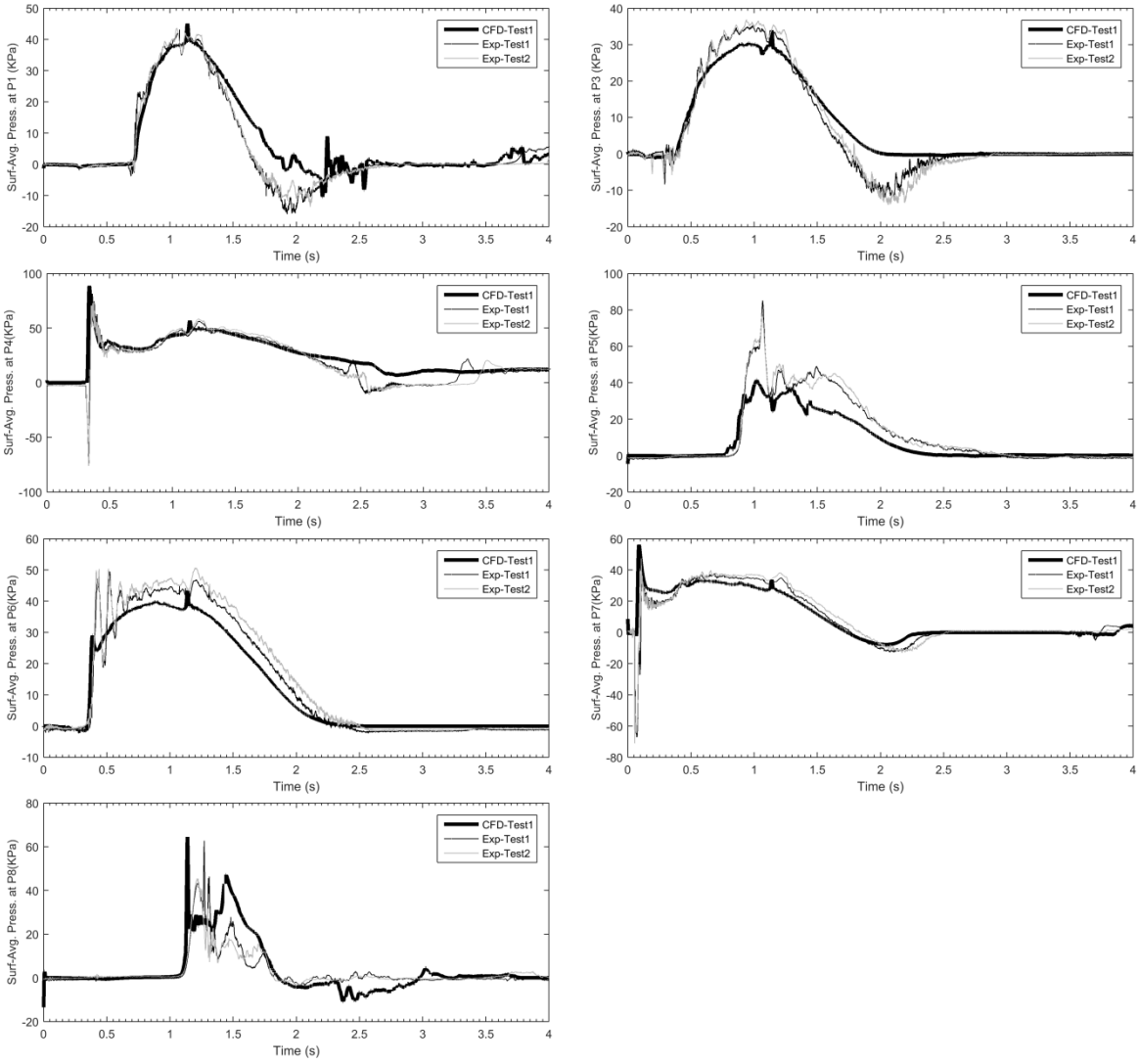

Figure 14

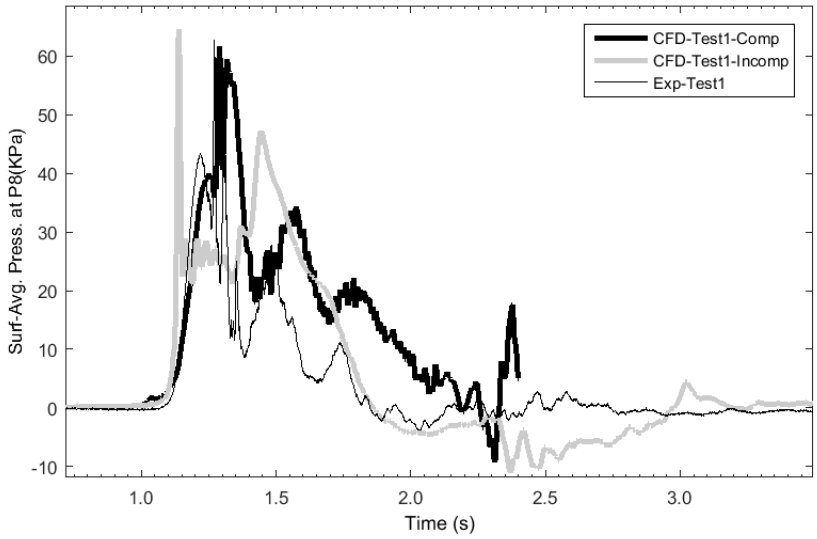

Figure 15

Tables

Table 1

Length overall, L	1.2m	
Mass	14.64 kg (for cases in wave headings of 60 and 90 deg) 15.00 kg (for cases in wave heading of 120 deg)	
Location of center of gravity COG from stern	0.565 m	
Location of center of gravity COG from keel	0.146 m	
Moments of Inertia (kg.m2)	For cases with wave headings: 60 and 90 degrees	For cases with wave heading of 120 degrees
Roll	0.135	0.138
Pitch	1.202	1.227
Yaw	1.172	1.201

Table 2

Case Number	Wave Heading [deg]	Wave Height H [m]	Wave Period T [s]	Location of hit point [HP]
1	90	0.75	2.58	0
2	90	0.75	2.58	1
3	90	0.75	2.58	2
4	90	0.75	2.58	3
5	60	0.75	2.58	0
6	60	0.75	2.58	1
7	60	0.75	2.58	2
8	60	0.75	2.58	3
9	120	0.75	2.58	0
10	120	0.75	2.58	1
11	120	0.75	2.58	2
12	120	0.75	2.58	3